Title

Micro-Computed Tomography-Based Three-Dimensional Kinematic Analysis During Lateral Bending for Spinal Fusion Assessment in a Rat Posterolateral Lumbar Fusion Model

Journal

Tissue Engineering Part C Methods, 20(7)

ISSN

1937-3384

Authors

Yamaguchi, Tomonori
Inoue, Nozomu
Sah, Robert L
et al.

Publication Date

2014-07-01

DOI

10.1089/ten.tec.2013.0439

Peer reviewed

TISSUE ENGINEERING: Part C
Volume 20, Number 7, 2014

DOI: 10.1089/ten.tec.2013.0439

Micro-Computed Tomography-Based Three-Dimensional Kinematic Analysis During Lateral Bending for Spinal Fusion Assessment in a Rat Posterolateral Lumbar Fusion Model

Tomonori Yamaguchi, MS,[1,2] Nozomu Inoue, MD, PhD,[2,3] Robert L. Sah, MD, ScD,[1,4] Yu-Po Lee, MD,[1] Alexander P. Taborek, BS,[1] Gregory M. Williams, PhD,[5] Timothy A. Moseley, PhD,[5] Won C. Bae, PhD,[6] and Koichi Masuda, MD[1]

Rat posterolateral lumbar fusion (PLF) models have been used to assess the safety and effectiveness of new bone substitutes and osteoinductive growth factors using palpation, radiography, micro-computed tomography (μCT), and histology as standard methods to evaluate spinal fusion. Despite increased numbers of PLF studies involving alternative bone substitutes and growth factors, the quantitative assessment of treatment efficacy during spinal motion has been limited. The purpose of this study was to evaluate the effect of spinal fusion on lumbar spine segment stability during lateral bending using a μCT-based three-dimensional (3D) kinematic analysis in the rat PLF model. Fourteen athymic male rats underwent PLF surgery at L4/5 and received bone grafts harvested from the ilium and femurs of syngeneic rats (Isograft, $n=7$) or no graft (Sham, $n=7$). At 8 weeks after the PLF surgery, spinal fusion was assessed by manual palpation, plain radiography, μCT, and histology. To determine lumbar segmental motions at the operated level during lateral bending, 3D kinematic analysis was performed. The Isograft group, but not the Sham group, showed spinal fusion on manual palpation (6/7), solid fusion mass in radiographs (6/7), as well as bone bridging in μCT and histological images (5/7). Compared to the Sham group, the Isograft group revealed limited 3D lateral bending angular range of motion and lateral translation during lateral bending at the fused segment where disc height narrowing was observed. This μCT-based 3D kinematic analysis can provide a quantitative assessment of spinal fusion in a rat PLF model to complement current gold standard methods used for efficacy assessment of new therapeutic approaches.

Introduction

Lumbar spinal fusion has been performed to relieve pain by immobilization of the degenerated and unstable spinal motion segment.[1] In this surgical procedure, the use of autologous bone grafting has historically remained the gold standard for achieving spinal fusion.[2] However, the potential for symptomatic pseudoarthrosis, a failure of stabilization of the fused segments, considered to be a common complication after spinal fusion, may result in continuous motion in a degenerated segment and persistent symptoms.[1,3] To augment bone healing and provide stability after spinal fusion, the development of grafting materials (e.g., demineralized bone matrix: DBM), osteoinductive growth factors (e.g., recombinant bone morphogenetic proteins: BMPs), and gene- or stem cell-based therapies has been introduced.[2,4,5]

To assess the efficacy of new therapeutic approaches, it is necessary to use several preclinical animal models.[6] In the initial development phase, noninstrumented posterolateral lumbar fusion (PLF) models in various species have commonly been used as clinically relevant models to evaluate the safety and efficacy of new bone substitutes as well as osteoinductive growth factors.[4,7–11] In these models, manual palpation, radiography, and histology have been the gold standard techniques for the evaluation of spinal fusion. The

Abstract was presented at the 2012 Orthopedic Research Society annual meeting (San Francisco, California).
[1]Department of Orthopaedic Surgery, School of Medicine, University of California, San Diego, La Jolla, California.
[2]Department of Biomedical Engineering, Graduate School of Life and Medical Sciences, Doshisha University, Kyoto, Japan.
[3]Department of Orthopedic Surgery, Rush University Medical Center, Chicago, Illinois.
[4]Department of Bioengineering, Jacobs School of Engineering, University of California, San Diego, La Jolla, California.
[5]Biologics, Nuvasive, Inc., San Diego, California.
[6]Department of Radiology, School of Medicine, University of California, San Diego, San Diego, California.

mechanical properties of the fusion mass have also been evaluated using destructive[8] or nondestructive[12,13] approaches. Furthermore, the application of micro-computed tomography (μCT) has improved the ability to determine bone fusion mass and bone bridging and has been widely used for structural assessment of spinal fusion.[4,13–27] However, quantitative approaches to assess functional spinal fusion during spinal motion have been limited.[28]

In the clinical environment, the effectiveness of spinal fusion has been studied using static and/or dynamic radiography,[29,30] CT,[31,32] and magnetic resonance imaging.[33] The recommended angular motion for successful spinal fusion using lateral radiographs in flexion and extension has varied from 0° to 5°.[30,34,35] Recent advances in imaging techniques have contributed the ability to analyze *in vivo* three-dimensional (3D) spine movements,[31–33] which may have the potential to precisely assess the performance of instrumentation and the effect of treatment on spine kinematics.[32]

We hypothesized that a 3D kinematic analysis, which has been developed to evaluate human spine motion after fusion,[31,36] can be adapted to assess spinal fusion in a rodent. The specific purpose of the current study was to determine the effect of spinal fusion on lumbar spine segments during lateral bending using a μCT-based 3D kinematic analysis in a rat PLF model compared to current gold standard methods.

Materials and Methods

Surgical operation

Fourteen 8-week-old athymic male rats (Harlan Laboratories, Inc., Indianapolis, IN), 200–250 g, were used with the authors' Institutional Animal Care and Use Committee approval. After the intraperitoneal administration of ketamine hydrochloride (75 mg/kg, Ketaset®; Fort Dodge Animal Health, Inc., Fort Dodge, IA) and xylazine (3 mg/kg, AnaSed®; Akorn, Inc., Lake Forest, IL), the rats were anesthetized with 1–2% isoflurane (Piramal Critical Care, Inc., Bethlehem, PA). PLF at L4/5 was performed under surgical microscopy. Through a single midline skin incision, the dorsal lumbar fascia was exposed and two paramedian fascial incisions (4 mm from the spinal processes) were made.[37] The transverse processes of L4 and L5 levels were decorticated with a stainless steel burr (1.5 mm head) until bleeding was observed. The wounds were irrigated with sterile saline to remove bone chips. Animals received 0.3 mL per side of bone graft (Isograft) harvested from two genetically similar (syngeneic) rats or no graft (Sham). For the Isograft surgery ($n=7$), morselized corticocancellous bone grafts ($2.5\times2.5\times2.5\,mm^3$) were harvested from the ilium and diaphysis of femurs of syngeneic rats. The Sham group received the same procedure with no delivery of graft materials ($n=7$). After placing the graft in both prepared sites ensuring direct contact with the transverse processes, the wound was closed in layers. The rats were kept *ad libitum* in their cage afterward. For postoperative pain management, buprenorphine hydrochloride (0.03 mg/kg, Buprenex®; Reckitt Benckiser Pharmaceuticals, Inc., Richmond, VA) was administered twice for the first postoperative day. At 8 weeks after the surgery, all animals were euthanized using CO_2 and lateral bending experiments were performed (Fig. 1).

Anteroposterior radiographic analysis

Anteroposterior (AP) radiography in each animal was performed immediately after the surgery, and at 2, 4, 6 and 8 weeks after the surgery (55 kV, 10 μAs) by digital radiography (Digital X-ray sensor NAOMI; 356 dpi, 71 μm pixel size; RF Co. Ltd., Nagano, Japan). Based on the presence of continuous bone formation between L4 and L5 transverse processes, two observers, blinded to the assigned treatments, graded the fusion mass as solid or not solid (Fig. 2A); the presence of bilateral solid fusion masses was considered fusion.

Manual palpation

After euthanizing animals at 8 weeks postoperatively, manual palpation was performed by two different observers,

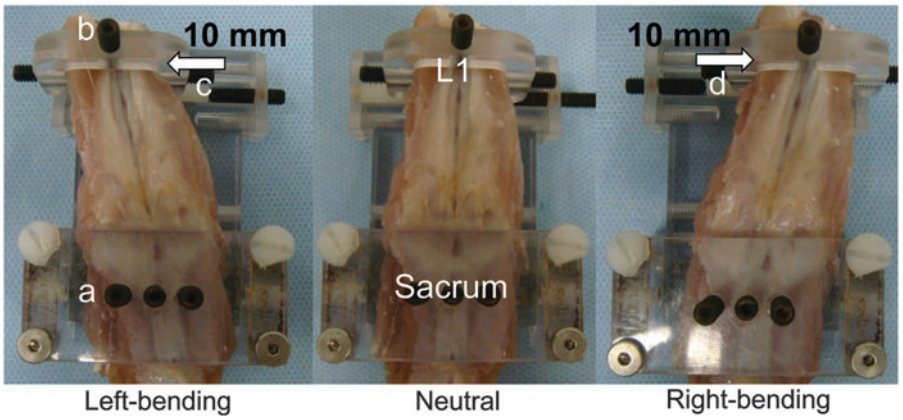

FIG. 1. An isolated rat lumbar spine was placed in the prone position on a micro-computed tomography (μCT)-compatible apparatus consisting of a sacral fixation jig (a) and a loading mechanism (b) to create different medial-lateral bending positions. The L1 vertebral body was displaced in the medial or lateral direction by applying a point displacement via a single set screw over the surrounding muscle layers, with anterior–posterior displacement being restricted by flat-ended spacers. The loading mechanism was set to three different positions (arrow): left-bending (c, +10.0 mm), neutral (0 mm), and right-bending (d, −10.0 mm). Color images available online at www.liebertpub.com/tec

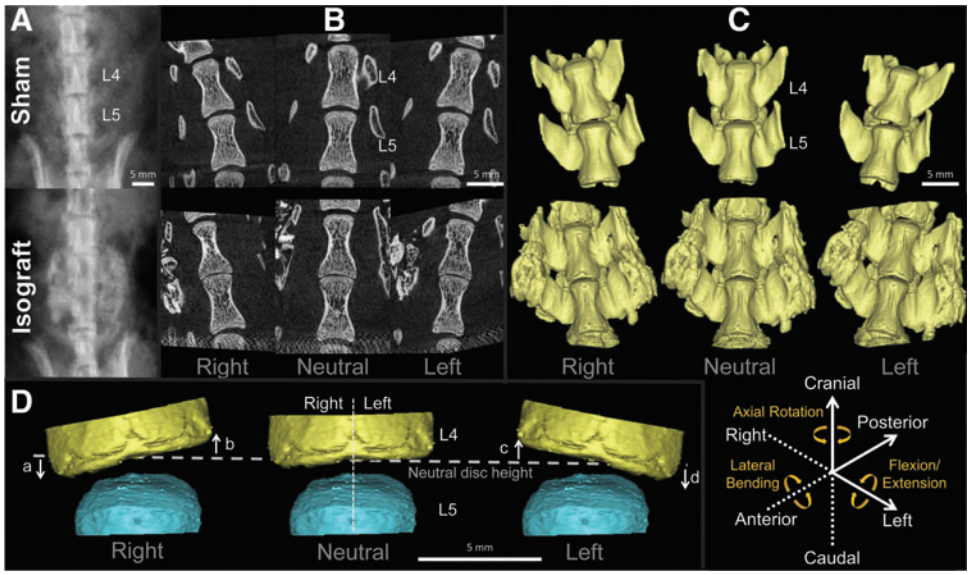

FIG. 2. **(A)** Eight weeks after posterolateral fusion surgery, animals were imaged, under anesthesia, using anteroposterior plain radiography (55 kV, 10 μAs). **(B)** Lumbar spines were harvested, placed into a lateral bending apparatus, and scanned using micro-computed tomography (μCT) in right-bending, neutral, and left-bending positions at a voxel size of 18 μm isotropic. **(C)** Corresponding three-dimensional (3D) models of L4 and L5 vertebral bodies were created for 3D kinematic analysis; the six degrees-of-freedom of segmental motion are shown (solid line: positive; broken line: negative). **(D)** Three-dimensional models of disc wedging: disc height changes in the right (a, c) and left (b, d) regions at each position (3D disc wedging = a + b + c + d). Scale bar = 5 mm. Color images available online at www.liebertpub.com/tec

blinded to the assigned treatments. The spinous processes at L4 and L5 were exposed with a minimal fascia incision, and intersegmental motion between the two levels was manually palpated using forceps. Based on the absence/presence of motion at the operated level, each sample was graded either as fusion or nonfusion.

Three-dimensional μCT analyses during lateral bending

μCT imaging. After manual palpation, lumbar spines with surrounding soft tissue and pelvis were carefully harvested from the rats and subjected to 3D μCT analyses at neutral, left- and right-bending positions. Displacement-controlled lateral bending of harvested spines was performed using a custom-bending apparatus (Fig. 1). The bending apparatus consisted of a sacral fixation jig and a loading mechanism to create different medial-lateral bending positions. After placing a dissected spine in the prone position, the sacrum was anchored tightly with three set screws to the fixation jig. The L1 vertebral body was displaced in the medial or lateral direction by applying a point displacement via a single set screw over the surrounding muscle layers, with anterior–posterior displacement being restricted by flat-ended spacers. Craniocaudal translation and axial, lateral, and flexion/extension rotations of the L1 were not constrained to allow cantilever bending of the specimen. The placement of each sample on the apparatus was confirmed by a μCT scout scan (SkyScan 1076; Bruker, Kontich, Belgium). The loading mechanism was set to three different positions: left-bending (+10.0 mm), neutral (0 mm), and right-bending (−10.0 mm), providing lateral bending of the whole lumbar spine with respect to the sacrum to L1 of ∼15° from neutral at each bending position. In each position, L4 and L5 vertebral bodies were imaged using the μCT scanner with the following parameters: (i) maximal potential (70 kV, 140 μA); (ii) 1.0-mm-thick aluminum filter; (iii) over 180° total rotation; (iv) 1.0° angular rotation step; and (v) a voxel size of 18 μm isotropic (Fig. 2B). Hydration was maintained by spraying specimens with saline before each μCT scan. The reconstructions, performed using the NRecon software package (SkyScan, Bruker, Kontich, Belgium), were based on the Feldkamp algorithm and resulted in axial grayscale images. Using DataViewer software (SkyScan, Bruker), two different observers, blinded to the assigned treatments, evaluated the presence of continuous bone bridging, without a gap, between L4 and L5 transverse processes (bone bridging)[10] in the neutral position and determined if the fusion mass was destructed during lateral bending; bilateral bone bridging was considered fusion. The ability to detect true positive (sensitivity) and true negative (specificity) of the conventional methods corresponding to μCT evaluation was calculated.

Three-dimensional kinematic analysis. To create 3D μCT-based vertebral models, the μCT images in the neutral, left- and right-bending positions were imported into a 3D reconstruction software package (Mimics 14.12; Materialise NV, Plymouth, MI, Fig. 2C). The threshold level to define the cortical shell of the vertebral body was selected and applied to all samples. First, transverse processes, and posterior elements and newly formed bone mass (only for the Isograft group) were manually removed to separate the vertebral body. After segmentation of L4 and L5 vertebral bodies, 3D point-cloud data sets were created of each vertebral body at each position, and 3D endplate point-cloud data sets were created based on the segmentation of the

endplate from each vertebral body. These procedures were performed by two independent orthopaedic researchers to evaluate model creation error for 3D kinematic and disc height analyses.

For 3D segmental movements with six degrees-of-freedom (three rotational and three translational segmental motions) at the operated level during lateral bending, 3D–3D rigid registration (the Volume-Merge method) was used after adjusting the scale for the difference in μCT resolution. The relative motion between L4 and L5 vertebral bodies was analyzed by considering the origin of the local coordinate system to be at the centroid of the cranial endplate of the L5 vertebral body for each motion segment as previously described (Fig. 2C).[31] The *x*-axis was set in an AP direction (posterior: positive). The *y*-axis was set in a lateral direction (left side: positive). The *z*-axis was set in a craniocaudal direction (cranial: positive). The total absolute value of rotation about the *x*-axis in lateral bending was defined as the *3D lateral bending angular range of motion (ROM)*. The averaged absolute value of rotation about the *y*-axis in lateral bending was defined as the *3D flexion/extension angular ROM* and that about the *z*-axis was defined as the *3D axial rotational angular ROM*. The averaged absolute value of translation distance along the *x*-axis in lateral bending was defined as the *3D AP translation*. The total absolute value of translation distance along the *y*-axis in lateral bending was defined as the *3D lateral translation*. The averaged absolute value of translation distance along the *z*-axis in lateral bending was defined as the *3D craniocaudal translation*.

Three-dimensional disc height measurements. The 3D disc height distribution was computed using a custom software.[31] The 3D mean disc height at the operated level was first calculated in the neutral position (*3D neutral disc height*), and the topographic zone analysis was then performed.[38] Each endplate point-cloud data point was converted from Cartesian coordinates to a spherical coordinate system with the centroid of the cranial endplate of the L5 vertebral body as the origin; the left and right regions were defined by an angular parameter in the spherical coordinate of each point from the posterior axis in the endplate (left region: $-180°$ to $0°$ and right region: $0°$ to $180°$). In lateral bending, the sum of the mean disc height that changes from the neutral position in the left and right region was defined as the *3D disc wedging* (Fig. 2D).

Two-dimensional radiographic analysis. To develop an assessment protocol for conventional radiography, the two-dimensional (2D) disc wedging angle was defined. First, using ImageJ (NIH, Bethesda, MD), virtual AP radiographs were created by combining coronal μCT images in left- and right-bending positions. On these radiographs, angles between the line along the caudal endplate of the L4 vertebral body and the cranial endplate of the L5 vertebral body at the left- and right-bending positions were measured. For each sample, the sum of the angles of left- and right-bending positions was calculated as the *2D disc wedging angle*.

Histology

After lateral bending examination, the tissues were fixed in 10% neutral-buffered formalin, decalcified, paraffin-embedded, and longitudinally sectioned (4 μm) in the sagittal plane along the L4 and L5 transverse processes at the center of the fusion mass; serial sections were stained with hematoxylin and eosin (H&E) or Masson's trichrome. The histological images were digitally captured using the Leica SCN400 Slide Scanner at 40× magnification (Leica Microsystems, Milton Keynes, United Kingdom). The presence of trabecular bone bridging between L4 and L5 transverse processes (bony fusion)[10] on two sections (one each of H&E and Masson's trichrome) was assessed by two different observers blinded to the assigned treatments.

Statistics

For comparisons between the Sham and Isograft groups, 2D disc wedging angle, 3D angular ROMs, 3D translations, 3D neutral disc height, and 3D disc wedging were analyzed using the unpaired *t*-test ($\alpha = 0.05$). Results are presented as mean ± standard deviation (SD). The observed data (fusion or nonfusion) were analyzed using the chi-square test. Correlations between 3D lateral bending angular ROM, 2D disc wedging angle, and 3D neutral disc height were assessed by the Pearson's correlation test. Statistical analyses were performed using StatView (Version 5.0; SAS Institute, Inc., Cary, NC). The standardized coefficient of variation (sCV) was also calculated to determine inter- and intra-observer errors of 2D radiographic and 3D μCT analyses.[39]

Results

Fusion rate by AP radiographs

Isograft animals revealed bilateral (6/7) and unilateral (1/7) solid fusion masses on AP radiographs at 8 weeks after the surgery, whereas none of the Sham animals showed bone formation at the L4/5 level (Tables 1 and 2 and Fig. 2A). The Isograft group showed a higher fusion rate than the Sham group ($p < 0.01$).

Table 1. Fusion Rate of Radiography, Manual Palpation, Micro-Computed Tomography, and Histology at 8 Weeks

	Fusion rate (fusion sample/total sample)			
Groups	*Radiography*	*Manual palpation*	*μCT*	*Histology*
Sham ($n = 7$)	0% (0/7)	0% (0/7)	0% (0/7)	0% (0/7)
Isograft ($n = 7$)	86% (6/7)[a]	86% (6/7)[a]	71% (5/7)[a]	71% (5/7)[a]

[a] $p < 0.01$, compared to the Sham group, chi-square test.
μCT, micro-computed tomography.

Table 2. The Results of Spinal Fusion Assessments in the Isograft Group ($N=7$) at 8 Weeks

Sample ID	*Radiography*	*Manual palpation*	*μCT*	*Histology*	*3D lateral bending*[a]	*3D neutral disc height*
Isograft#01	Nonfusion	Nonfusion	Nonfusion	Fibrous union	1.08°	0.33 mm
Isograft#02	Fusion	Fusion	Fusion	Bony fusion	0.27°	0.22 mm
Isograft#03	Fusion	Fusion	Nonfusion	Fibrous union	3.64°	0.44 mm
Isograft#04	Fusion	Fusion	Fusion	Bony fusion	0.71°	0.27 mm
Isograft#05	Fusion	Fusion	Fusion	Bony fusion	0.37°	0.20 mm
Isograft#06	Fusion	Fusion	Fusion	Bony fusion	0.25°	0.30 mm
Isograft#07	Fusion	Fusion	Fusion	Bony fusion	0.7°	0.24 mm

[a]Three-dimensional lateral bending angular range of motion.
3D, three-dimensional.

Fusion rate by manual palpation

At 8 weeks after the surgery, all animals in the Sham group showed motion at the operated level (Table 1). The absence of motion at the fused segment was observed in six animals in the Isograft group (6/7) (Table 1); one animal showed minimal motion and intermediate fusion (1/7) (Table 2), unlike that seen in the Sham group. The fusion rate in the Isograft group was significantly higher than that in the Sham group ($p<0.01$).

Qualitative bone mass assessment by μCT images

On μCT images in the neutral position, bone bridging was not observed in the Sham group (Table 1 and Fig. 3A). In the Isograft group, bilateral bone bridging at the operated level was observed in five animals (5/7) (Tables 1 and 2 and Fig. 3B) with one animal showing only unilateral bone bridging (1/7) (Fig. 3C), and another animal revealing gaps in fusion mass in a bilateral fashion (1/7) (Fig. 3D). When comparing μCT images at the neutral position and at the bending positions, the fusion mass appeared intact.

Three-dimensional segmental motion

The 3D lateral bending angular ROM in the Isograft group (1.00 ± 1.20°) was significantly lower than that in the Sham group (12.44 ± 2.10°, $p<0.0001$, Table 2 and Fig. 4A). The 3D flexion/extension angular ROM caused by coupled motions, defined as segmental movement independent of lateral bending, in the Isograft group (0.38 ± 0.25°) was lower compared to the Sham group (1.19 ± 0.75°, $p<0.05$). The 3D axial angular ROM also caused by coupled motions associated with lateral bending in the Isograft group (0.80 ± 0.44°) was significantly lower than that in the Sham group (1.74 ± 0.84°, $p<0.05$).

The 3D lateral translation in the Isograft group (0.05 ± 0.04 mm) was significantly lower than that in the Sham group (0.14 ± 0.08 mm). There were no significant differences between the groups in the 3D AP and craniocaudal translations caused by coupled motions associated with lateral bending (data not shown). The calculated inter- and intra-observer errors of the 3D kinematic analysis were 2.0% and 2.2% (sCV), respectively.

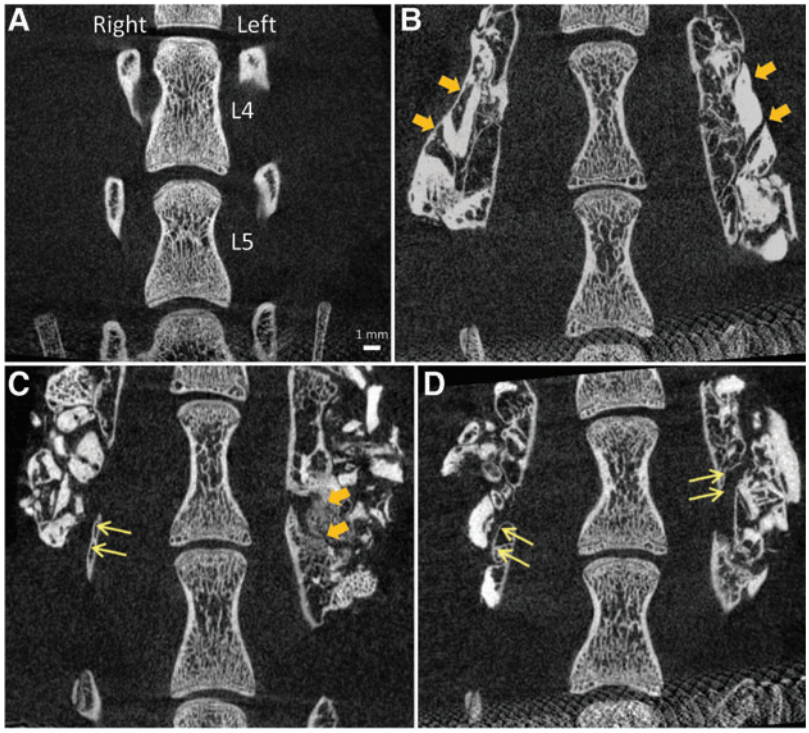

FIG. 3. Anteroposterior micro-computed tomography (μCT) image assessment for bone bridging in the neutral position. Representative coronal μCT images of L4 and L5 vertebrae and transverse processes from a Sham animal **(A)** and Isograft animals with bilateral bone bridging **(B)**, unilateral bone bridging (Isograft#01, **C**), and no bone bridging (Isograft#03, **D**). Thick arrows show continuous bone bridging and thin arrows indicate the presence of a gap in the fusion mass. Scale bar = 1 mm. Color images available online at www.liebertpub.com/tec

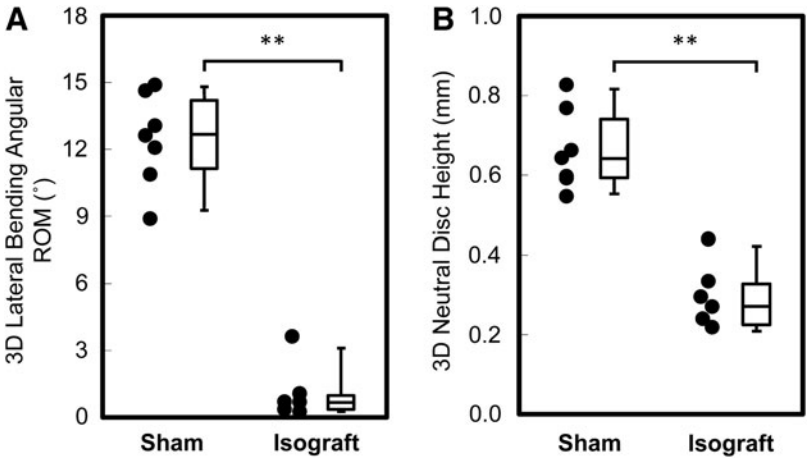

FIG. 4. Box plots show three-dimensional (3D) lateral bending angular range of motion (ROM) **(A)** and 3D neutral disc height calculated using 3D vertebral models **(B)**. In the Isograft group, limited 3D lateral bending angular ROM **(A)** and 3D neutral disc height narrowing **(B)** are observed at the fused level compared to the Sham group. $^{**}p < 0.0001$, unpaired *t*-test.

Three-dimensional disc height

The 3D neutral disc height in the Isograft group (0.29 ± 0.08 mm) was significantly lower than that in the Sham group (0.66 ± 0.10 mm, $p < 0.0001$, Table 2 and Fig. 4B). This 3D neutral disc height narrowing at the fused level was strongly correlated with the 3D lateral bending angular ROM (Pearson's correlation = 0.90, $p < 0.0001$). The 3D disc wedging in the Isograft group (0.08 ± 0.03 mm) revealed limited disc wedging compared to the Sham group (0.31 ± 0.10 mm, $p < 0.05$) (Fig. 5). The calculated inter- and intra-observer errors of the 3D disc wedging analysis were 4.6% and 5.9% (sCV), respectively.

Two-dimensional disc wedging angle

The 2D disc wedging angle in the Isograft group ($1.63 \pm 1.13°$) was significantly lower than that in the Sham group ($10.18 \pm 3.73°$, $p < 0.0001$). The 2D disc wedging angle was positively correlated with the 3D lateral bending angular ROM (Pearson's correlation = 0.87, $p < 0.0001$). The calculated inter- and intra-observer errors of the 2D disc wedging angle assessment were 5.1% and 5.1% (sCV), respectively.

Histological assessment

In the histological evaluations with H&E and Masson's trichrome staining, no bone formation between the L4 and L5 transverse processes was observed in the Sham group (Fig. 6A, D). In the Isograft group, five animals achieved bony fusion (5/7) (Fig. 6B, E). The other two animals displayed fibrous tissue filling a gap in the fusion mass that was considered fibrous union (2/7) (Fig. 6C, F). The histological observations for nonfused samples agreed with the μCT image findings.

Sensitivity and specificity of spinal fusion assessments

Compared to the μCT evaluation, the sensitivity of manual palpation, radiography, and histology was all 100%, and the specificity was 89%, 89%, and 100%, respectively. There were no interobserver differences in all spinal fusion assessments.

Discussion

This study was able to precisely and reproducibly evaluate the effect of spinal fusion on lumbar spine segment stability in a rat PLF model by combining the 3D kinematic

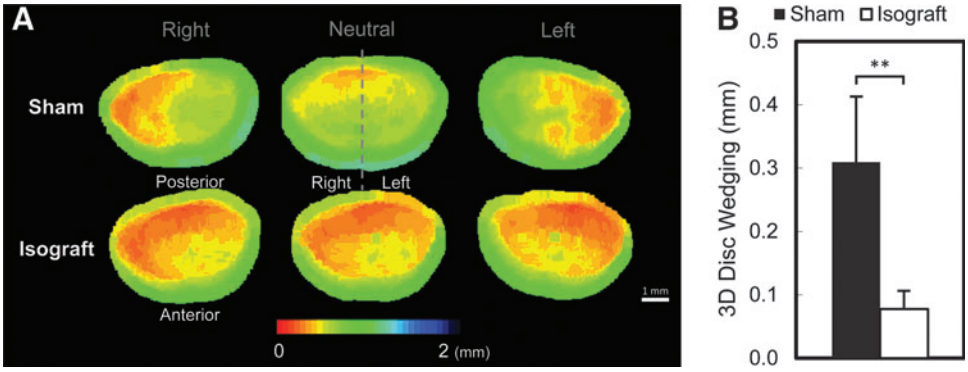

FIG. 5. **(A)** Disc height distribution (color bar range: red = 0 mm; blue = 2 mm disc height), in representative Sham (top row) and Isograft (bottom row) samples in right-bending (left column), neutral (center column), and left-bending (right column) positions. The Isograft group shows disc height narrowing in neutral compared to the Sham group. **(B)** Three-dimensional (3D) disc wedging is determined during lateral bending; 3D disc wedging in the Isograft group is less than that in the Sham group. The data are presented as mean ± standard deviation (SD). $^{**}p < 0.0001$, unpaired *t*-test. Scale bar = 1 mm. Color images available online at www.liebertpub.com/tec

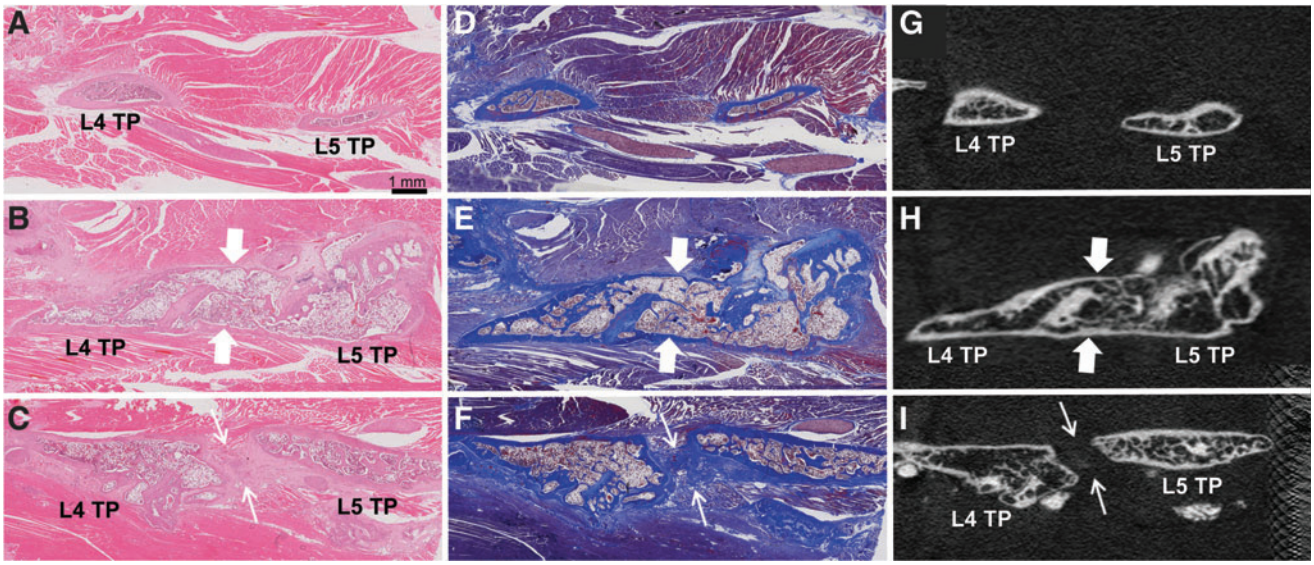

FIG. 6. Para-sagittal histological images of hematoxylin and eosin (H&E) (left column) and Masson's trichrome (middle column) with corresponding micro-computed tomography (μCT) images (right column) between the L4 and L5 transverse processes (TPs). Representative histological and μCT images show no bone formation from a Sham animal **(A, D, G)**, bony fusion from an Isograft animal **(B, E, H**: thick arrow**)**, and fibrous union from Isograft#03 **(C, F, I**: thin arrow**)**. Histological slides were scanned with a Leica SCN400 Slide Scanner (40×), and μCT images were obtained using the SkyScan 1076 (18 μm). Scale bar = 1 mm. Color images available online at www.liebertpub.com/tec

analysis developed to evaluate human spinal motion[31,36] and μCT images during lateral bending. In addition, 3D disc height measurements revealed disc height narrowing and limited disc wedging with lateral bending at the fused level. Compared to standard methods, these 3D μCT analyses can provide a quantitative assessment for the functional efficacy of new bone substitutes and osteoinductive growth factors in a rat PLF model.

Clinically, flexion/extension radiography has been widely used for spinal fusion assessment.[29] The lateral bending approach has also been considered a valuable clinical method for segmental motion analysis.[40,41] In our study, the lateral bending approach with displacement control was chosen for several reasons. First, it allows creation of different spinal positions within the limited scanning space of the μCT scanner; the flexion/extension approach would require more space for displacement than the lateral bending approach under the same loading condition.[42] Second, the lateral bending approach minimizes the error caused by interference from the presence of bone fusion mass in the flexion/extension plane of 2D radiographic analysis. Within the range of displacement applied in this study, the two experimental groups (Sham and Isograft) were clearly distinguished by the 3D kinematic analysis, with no evidence of destruction of fusion mass.

The accuracy of the Volume-Merge method used in the 3D analysis was reported as 0.2° in rotation and 0.1 mm in translation using a clinical CT scanner with a resolution of ~0.5 mm.[36] After adjusting the scale for μCT resolution, the accuracy in translation is expected to be 3.6 μm in the current study, although the actual accuracy needs to be validated in the μCT system. The present study also applied 3D disc height measurements developed in clinical CT 3D models to the rat PLF model using the μCT system.[31]

When 2D and 3D analyses were compared, the results of the present study showed a significant correlation between 2D disc wedging angle and 3D lateral bending angular ROM. Two-dimensional radiographic analyses are relatively easy to perform and cost-effective, but, importantly, vertebral orientation and differences in marking landmark points may affect the results.[29,31,42] The 3D μCT analysis used in our study showed better interobserver (sCV: 2.0%) and intra-observer (sCV: 2.2%) reproducibility than those of the 2D radiographic analysis (sCV: 5.1% for both) and was independent of vertebral orientation, suggesting that the error of vertebral model creation was minimized.

There have been several studies analyzing lumbar spine segments using radiographic and μCT imaging techniques in small animals.[28,42] Dewan *et al.* evaluated the mechanical integrity of spinal fusion during flexion/extension conditions using μCT in mice and showed decreased intervertebral motion in the fusion group compared to that in the control group.[28] However, these authors indicated that determining the significance in the variability of fusions observed with μCT can be challenging.[28] The current study demonstrated that, in the Isograft group, the 3D lateral bending angular ROMs in bilateral fusion samples were as small as 0.71° or less, while those in unilateral fusion (Isograft#01) or nonfusion (Isograft#03) samples were 1.08° and 3.64°, respectively. This quantitative information for the status of intermediate spinal fusion, such as observed in Isografts#01 and #03, supports the usefulness of the 3D kinematic analysis. It may be possible for us to differentiate characteristics of nonfusion, fibrous fusion, and solid bone fusion using this technique; further studies using various materials may be worthy to conduct.

Manual palpation has been well established to distinguish fusion mass in animals.[6,8,10,11] AP radiographic observation

has also been used to follow-up the evidence of bone formation at multiple time points.[8,10] The current study, however, showed lower specificity with a false-positive result (Isograft#03) on both manual palpation and radiographic assessments when compared to μCT evaluation. Importantly, forces applied during the manual palpation procedure are not well documented and standardized among researchers; the procedure with excess forces can cause micro-cracks or separation from the transverse processes if the fusion strength is not sufficient. Histological images provided extensive information on the fusion mass to characterize bony fusion or fibrous union using different staining techniques.[11] Although our histological results agreed with our μCT assessment (100%) with careful definition of the specimen preparation plane, histology has the potential to miss bony fusion due to out-of-plane bone bridging.[11,16] Limitations of the μCT assessment, however, should be considered as well. We confirmed no destruction of the newly formed bone, potentially caused by manual palpation and/or lateral bending procedures, using μCT images. However, a resolution of 18 μm used in the current study may not be high enough to detect potential micro-cracks caused by these procedures. On the other hand, connectivity of the newly formed bone across the gap was shown even in the nonfusion cases by voxel-based connectivity analysis in the 3D μCT model (data not shown), which appears to be caused by the voxel(s) at the gap due to noise and/or possible lower gray level threshold setting. The optimal combination of various spinal fusion assessments[11] should be used to accurately determine safety and efficacy of alternative bone substitute and growth factors.

Interestingly, the current study showed disc height narrowing at the fused level at 8 weeks after the surgery that correlated with an achievement of fusion. Although the mechanism of disc height narrowing is unclear, one can hypothesize that it was caused by shrinkage of the fusion mass during new bone formation and the remodeling process, or, alternatively, a compositional change due to non-loading condition in the intervertebral disc after fusion.[43] Further study using *in vivo* μCT scans at multiple time points may give us an insight on disc narrowing associated with spine fusion.

In addition, the 3D kinematic analysis detected limited flexion/extension and axial rotations at the fused segment, defined as coupled motions during lateral bending. The measurement of coupled motion is necessary to accurately evaluate spinal fusion.[31] Another important finding is that residual segmental movement at the fused level was found using the 3D μCT analyses. Residual motion at the fusion level has been reported in clinical cases in spinal fusion[44]; the acceptable value for spinal fusion by the US Food and Drug Administration is an angular motion $< 5°$ on flexion/extension radiographs.[35] To the best of our knowledge, this is the first study to demonstrate the presence of residual motion of newly formed bone in an animal spinal fusion model. Our rat PLF model showed that residual motion was $< 0.71°$ in bilateral solid fusion levels defined by μCT images. Bono *et al.* analyzed segmental movement at simulated fused levels using finite element analysis[34] as well as biomechanical testing[45] and demonstrated that a solid fusion mass has the potential to permit residual motion due to the elastic deformity of bone. Therefore, based on our micro-structure evaluation, residual motion seen in solid fusion levels may be explained by such elastic deformity of newly formed bone. Because the current study focused on μCT-based 3D kinematic analysis and a comparison was made only between the Sham group and the Isograft group, parameters of the solid fusion mass, such as volume, density, and geometry of the newly formed bone, which can be measured by μCT images and used for the elastic deformity analyses of the fusion models, were not assessed. Further comparisons of residual motion between this model and human clinical fusion may be of interest.

Conclusion

This μCT-based 3D kinematic analysis during lateral bending in a rat PLF model has the ability to provide quantitative information for the functional effectiveness of new bone substitute and osteoinductive growth factors designed to improve spinal fusion; this technique will complement conventional assessments of spinal fusion. Using this 3D kinematic analysis, motion was diminished with the formation of fusion masses composed of newly formed bone, although some residual motion was present even with fusion. Furthermore, it was found that disc height narrowing at the fused level can be indicative of the achievement of spinal fusion.

Acknowledgments

T.Y. was a recipient of Young Researcher Overseas Visits Program for Vitalizing Brain Circulation (Japan Society for the Promotion of Science). The authors thank Rachit Parikh, M.S., for his assistance with the design and development of the spine jig.

Disclosure Statement

This research was partially supported by an institutional grant from Nuvasive, Inc.

References

1. Lee, C.K., and Langrana, N.A. Lumbosacral spinal fusion. A biomechanical study. Spine **9,** 574, 1984.
2. Vaccaro, A.R., Chiba, K., Heller, J.G., Patel, T., Thalgott, J.S., Truumees, E., Fischgrund, J.S., Craig, M.R., Berta, S.C., and Wang, J.C. Bone grafting alternatives in spinal surgery. Spine J **2,** 206, 2002.
3. Deyo, R.A., Ciol, M.A., Cherkin, D.C., Loeser, J.D., and Bigos, S.J. Lumbar spinal fusion. A cohort study of complications, reoperations, and resource use in the Medicare population. Spine **18,** 1463, 1993.
4. Zhu, W., Rawlins, B.A., Boachie-Adjei, O., Myers, E.R., Arimizu, J., Choi, E., Lieberman, J.R., Crystal, R.G., and Hidaka, C. Combined bone morphogenetic protein-2 and −7 gene transfer enhances osteoblastic differentiation and spine fusion in a rodent model. JBMR **19,** 2021, 2004.
5. Gottfried, O.N., and Dailey, A.T. Mesenchymal stem cell and gene therapies for spinal fusion. Neurosurgery **63,** 380, 2008.
6. Schimandle, J.H., and Boden, S.D. Spine update. The use of animal models to study spinal fusion. Spine **19,** 1998, 1994.
7. Morone, M.A., and Boden, S.D. Experimental posterolateral lumbar spinal fusion with a demineralized bone matrix gel. Spine **23,** 159, 1998.

8. Boden, S.D., Schimandle, J.H., and Hutton, W.C. An experimental lumbar intertransverse process spinal fusion model. Radiographic, histologic, and biomechanical healing characteristics. Spine **20,** 412, 1995.
9. Salamon, M.L., Althausen, P.L., Gupta, M.C., and Laubach, J. The effects of BMP-7 in a rat posterolateral intertransverse process fusion model. J Spinal Disord Tech **16,** 90, 2003.
10. Wang, J.C., Kanim, L.E., Yoo, S., Campbell, P.A., Berk, A.J., and Lieberman, J.R. Effect of regional gene therapy with bone morphogenetic protein-2-producing bone marrow cells on spinal fusion in rats. J Bone Joint Surg Am **85-A,** 905, 2003.
11. Drespe, I.H., Polzhofer, G.K., Turner, A.S., and Grauer, J.N. Animal models for spinal fusion. Spine J **5,** 209S, 2005.
12. Erulkar, J.S., Grauer, J.N., Patel, T.C., and Panjabi, M.M. Flexibility analysis of posterolateral fusions in a New Zealand white rabbit model. Spine **26,** 1125, 2001.
13. Park, B.H., Song, K.J., Yoon, S.J., Park, H.S., Jang, K.Y., Zhou, L., Lee, S.Y., Lee, K.B., and Kim, J.R. Acceleration of spinal fusion using COMP-angiopoietin 1 with allografting in a rat model. Bone **49,** 447, 2011.
14. Morisue, H., Matsumoto, M., Chiba, K., Matsumoto, H., Toyama, Y., Aizawa, M., Kanzawa, N., Fujimi, T.J., Uchida, H., and Okada, I. A novel hydroxyapatite fiber mesh as a carrier for recombinant human bone morphogenetic protein-2 enhances bone union in rat posterolateral fusion model. Spine (Phila Pa 1976) **31,** 1194, 2006.
15. Abe, Y., Takahata, M., Ito, M., Irie, K., Abumi, K., and Minami, A. Enhancement of graft bone healing by intermittent administration of human parathyroid hormone (1–34) in a rat spinal arthrodesis model. Bone **41,** 775, 2007.
16. Lu, S.S., Zhang, X., Soo, C., Hsu, T., Napoli, A., Aghaloo, T., Wu, B.M., Tsou, P., Ting, K., and Wang, J.C. The osteoinductive properties of Nell-1 in a rat spinal fusion model. Spine J **7,** 50, 2007.
17. Hsu, W.K., Wang, J.C., Liu, N.Q., Krenek, L., Zuk, P.A., Hedrick, M.H., Benhaim, P., and Lieberman, J.R. Stem cells from human fat as cellular delivery vehicles in an athymic rat posterolateral spine fusion model. J Bone Joint Surg Am **90,** 1043, 2008.
18. Miyazaki, M., Sugiyama, O., Zou, J., Yoon, S.H., Wei, F., Morishita, Y., Sintuu, C., Virk, M.S., Lieberman, J.R., and Wang, J.C. Comparison of lentiviral and adenoviral gene therapy for spinal fusion in rats. Spine **33,** 1410, 2008.
19. Miyazaki, M., Sugiyama, O., Tow, B., Zou, J., Morishita, Y., Wei, F., Napoli, A., Sintuu, C., Lieberman, J.R., and Wang, J.C. The effects of lentiviral gene therapy with bone morphogenetic protein-2-producing bone marrow cells on spinal fusion in rats. J Spinal Disord Tech **21,** 372, 2008.
20. Lopez, M.J., McIntosh, K.R., Spencer, N.D., Borneman, J.N., Horswell, R., Anderson, P., Yu, G., Gaschen, L., and Gimble, J.M. Acceleration of spinal fusion using syngeneic and allogeneic adult adipose derived stem cells in a rat model. J Orthop Sug Res **27,** 366, 2009.
21. Seo, H.S., Jung, J.K., Lim, M.H., Hyun, D.K., Oh, N.S., and Yoon, S.H. Evaluation of spinal fusion using bone marrow derived mesenchymal stem cells with or without Fibroblast Growth Factor-4. J Korean Neurosurg Soc **46,** 397, 2009.
22. Hsu, W.K., Polavarapu, M., Riaz, R., Roc, G.C., Stock, S.R., Glicksman, Z.S., Ghodasra, J.H., and Hsu, E.L. Nanocomposite therapy as a more efficacious and less inflammatory alternative to bone morphogenetic protein-2 in a rodent arthrodesis model. J Orthop Surg Res **29,** 1812, 2011.
23. Lee, J.H., and Jeong, B.O. The effect of hyaluronate-carboxymethyl cellulose on bone graft substitute healing in a rat spinal fusion model. J Korean Neurosurg Soc **50,** 409, 2011.
24. Abbah, S.A., Liu, J., Lam, R.W., Goh, J.C., and Wong, H.K. *In vivo* bioactivity of rhBMP-2 delivered with novel polyelectrolyte complexation shells assembled on an alginate microbead core template. J Control Release **162,** 364, 2012.
25. Okamoto, S., Ikeda, T., Sawamura, K., Nagae, M., Hase, H., Mikami, Y., Tabata, Y., Matsuda, K., Kawata, M., and Kubo, T. Positive effect on bone fusion by the combination of platelet-rich plasma and a gelatin beta-tricalcium phosphate sponge: a study using a posterolateral fusion model of lumbar vertebrae in rats. Tissue Eng Part A **18,** 157, 2012.
26. Abbah, S.A., Liu, J., Goh, J.C., and Wong, H.K. Enhanced control of *in vivo* bone formation with surface functionalized alginate microbeads incorporating heparin and human bone morphogenetic protein-2. Tissue Eng Part A **19,** 350, 2013.
27. Koerner, J.D., Yalamanchil, P., Munoz, W., Uko, L., Chaudhary, S.B., Lin, S.S., and Vives, M.J. The effects of local insulin application to lumbar spinal fusions in a rat model. Spine J **13,** 22, 2013.
28. Dewan, A.K., Dewan, R.A., Calderon, N., Fuentes, A., Lazard, Z., Davis, A.R., Heggeness, M., Hipp, J.A., and Olmsted-Davis, E.A. Assessing mechanical integrity of spinal fusion by *in situ* endochondral osteoinduction in the murine model. J Orthop Surg Res **5,** 58, 2010.
29. Goldstein, C., and Drew, B. When is a spine fused? Injury **42,** 306, 2011.
30. Santos, E.R., Goss, D.G., Morcom, R.K., and Fraser, R.D. Radiologic assessment of interbody fusion using carbon fiber cages. Spine **28,** 997, 2003.
31. Watanabe, S., Inoue, N., Yamaguchi, T., Hirano, Y., Espinoza Orias, A.A., Nishida, S., Hirose, Y., and Mizuno, J. Three-dimensional kinematic analysis of the cervical spine after anterior cervical decompression and fusion at an adjacent level. Eur Spine J **21,** 946, 2012.
32. Anderst, W.J., Baillargeon, E., Donaldson, W.F., 3rd, Lee, J.Y., and Kang, J.D. Validation of a noninvasive technique to precisely measure *in vivo* three-dimensional cervical spine movement. Spine **36,** E393, 2011.
33. Li, G., Wang, S., Passias, P., Xia, Q., and Wood, K. Segmental *in vivo* vertebral motion during functional human lumbar spine activities. Eur Spine J **18,** 1013, 2009.
34. Bono, C.M., Khandha, A., Vadapalli, S., Holekamp, S., Goel, V.K., and Garfin, S.R. Residual sagittal motion after lumbar fusion: a finite element analysis with implications on radiographic flexion-extension criteria. Spine **32,** 417, 2007.
35. Guidance Document for the Preparation of IDEs for Spinal Systems. Available at www.fda.gov/downloads/MedicalDevices/DeviceRegulationandGuidance/GuidanceDocuments/ucm073772.pdf (Accessed 2000 Jan 13)
36. Ochia, R.S., Inoue, N., Renner, S.M., Lorenz, E.P., Lim, T.H., Andersson, G.B.J., and An, H.S. Three-dimensional *in vivo* measurement of lumbar spine segmental motion. Spine (Phila Pa 1976) **31,** 2073, 2006.
37. Wiltse, L.L., and Spencer, C.W. New uses and refinements of the paraspinal approach to the lumbar spine. Spine **13,** 696, 1988.
38. Simon, P., Espinoza Orias, A.A., Andersson, G.B.J., An, H.S., and Inoue, N. *In vivo* topographic analysis of lumbar

facet joint space width distribution in healthy and symptomatic subjects. Spine **37,** 1058, 2012.
39. Orgee, J.M., Foster, H., McCloskey, E.V., Khan, S., Coombes, G., and Kanis, J.A. A precise method for the assessment of tibial ultrasound velocity. Osteoporos Int **6,** 1, 1996.
40. Dvorak, J., Panjabi, M.M., Chang, D.G., Theiler, R., and Grob, D. Functional radiographic diagnosis of the lumbar spine. Flexion-extension and lateral bending. Spine **16,** 562, 1991.
41. Ohtori, S., Yamashita, M., Inoue, G., Yamauchi, K., Koshi, T., Suzuki, M., Takaso, M., Orita, S., Eguchi, Y., Ochiai, N., Kishida, S., Mimura, M., Yanagawa, N., Ishikawa, T., Arai, G., Miyagi, M., Kamoda, H., Aoki, Y., Kuniyoshi, K., Nakamura, J., and Takahashi, K. Rotational hypermobility of disc wedging using kinematic CT: preliminary study to investigate the instability of discs in degenerated scoliosis in the lumbar spine. Eur Spine J **19,** 989, 2010.
42. Cunningham, M.E., Beach, J.M., Bilgic, S., Boachie-Adjei, O., van der Meulen, M.C., and Hidaka, C. *In vivo* and *in vitro* analysis of rat lumbar spine mechanics. Clin Orthop Relat Res **468,** 2695, 2010.
43. Taylor, T.K., Ghosh, P., Braund, K.G., Sutherland, J.M., and Sherwood, A.A. The effect of spinal fusion on intervertebral disc composition: an experimental study. J Surg Res **21,** 91, 1976.
44. Stauffer, R.N., and Coventry, M.B. Posterolateral lumbar-spine fusion. Analysis of Mayo Clinic series. J Bone Joint Surg **54,** 1195, 1972.
45. Bono, C.M., Bawa, M., White, K.K., Mahar, A., Vives, M., Kauffman, C., and Garfin, S.R. Residual motion on flexion-extension radiographs after simulated lumbar arthrodesis in human cadavers. J Spinal Disord Tech **21,** 364, 2008.

Address correspondence to:
Koichi Masuda, MD
Department of Orthopaedic Surgery
School of Medicine
University of California
9500 Gilman Drive, MC 0863
La Jolla, CA 92093-0863

E-mail: komasuda@ucsd.edu

Received: July 18, 2013
Accepted: November 5, 2013
Online Publication Date: January 9, 2014